DIFFERENTIAL ROTATION IN A SOLAR-DRIVEN QUASI-AXISYMMETRIC CIRCULATION

H. G. MAYR, I. HARRIS, and K. L. CHAN*

NASA/Goddard Space Flight Center, Laboratory for Planetary Atmospheres, Greenbelt, Maryland, U.S.A.

(Received 20 March, 1984)

Abstract. We consider the concept of a quasi-axisymmetric circulation to explore the global scale dynamics of planetary atmospheres. The momentum and energy transport processes in the smaller scales are formulated in terms of anisotropic eddy diffusion. In the early work of Williams and Robinson (1973) these concepts have been introduced to describe the Jovian circulation. Our study differs in that we adopt a spectral model (with vector spherical harmonics) and consider a linear system; we are also examining a different parameter regime. The troposphere of Jupiter is assumed to be weakly convectively unstable, and the circulation is driven by the fundamental component of solar differential heating with a broad maximum at the equator. Mode coupling arising from the Coriolis action is considered in self consistent form, and momentum and energy are allowed to cascade from lower to higher order modes. With a limited number of spherical harmonics, up to order 40, and with homogeneous boundary conditions, the conservation equations are integrated between the 25 and 10^{-5} bar pressure levels. In addition, a simplified single layer model is discussed which, even though heuristic in nature, elucidates and complements the numerical results. Our analysis leads to the following conclusions: (a) For a negative stability, $S_0 = \partial T_0/\partial r + \Gamma$, the energy transports arising from large scale advection by the meridional circulation can amplify the response to the external heating. This crucially depends on the latitudinal structure of the circulation, so that banded wind fields with equatorial zonal jets are preferentially excited. (b) With a negative stability of order $S_0 \sim -10^{-6}$ K cm^{-1}, the computed number of positive (and negative) zonal jets is similar to that observed on Jupiter. (c) The observed magnitudes in the zonal wind velocities require that the vertical eddy diffusion coefficient is of the order $K_r \sim 3 \times 10^5$ cm^2 s^{-1}, which in turn is consistent with the observed outward flux of energy from the planetary interior ($F \propto K_r S_0$); this diffusion rate is also of the right order of magnitude to obey mixing length theory. (d) The ratio between the horizontal and vertical eddy diffusion coefficients (relative mixing factor) is of critical importance. If it is too large ($\gg 10^5$), differential rotation or alternating zonal jets cannot be maintained; if it is too small ($\ll 10^4$), the equator tends to corotate. The intermediate value of order $R \sim 5 \times 10^4$ is again consistent with mixing length theory. (e) With the above constraints on the transport coefficients, the flow is quasi-geostrophic. (f) The meridional circulation is multicellular and of the Ferrel–Thomson type. It is consistent with the observed cloud striations in the Jovian atmosphere. (g) In the stable stratosphere at higher altitudes the fundamental component, directly driven by the Sun, dominates. The circulation degenerates, and broad, positive zonal jets develop at middle latitudes, resembling the observed wind field in the visible cloud cover of the Venus atmosphere.

1. Introduction

In the mean circulation of planetary atmospheres there are two related phenomena: (1) the rigid shell component (or global average) of superrotation and (2) the (latitudinal) differential rotation. On Venus, the rigid shell superrotation dominates (e.g., Schubert

* Applied Research Corporation, Landover, Maryland, U.S.A.

Earth, Moon, and Planets **30** (1984) 245–274. 0167-9295/84/0303-0245$04.50.

et al., 1980). On Jupiter and Saturn, banded wind fields with equatorial jets are prominent (Smith *et al.*, 1979a, b, 1981).

On the basis of the work of Biermann (1951), Durney and Roxburgh (1971) and Rüdiger (1980) and in particular that of Williams and Robinson (1973) and Gierasch (1975), we had shown in an earlier paper (Mayr and Harris, 1983; hereafter referred to as Paper I) that, under anisotropic eddy diffusion, the solar differential heating at low latitudes can drive the four day superrotation on Venus. With a Prandtl number of one, the adopted ratio of order 10^5 between the horizontal and vertical eddy diffusion coefficients was found to be of critical importance. A much larger value would significantly dampen the latitudinal temperature contrast required to sustain the observed superrotation rate; a much smaller value would not be able to sustain the observed motions near the equator. This required anisotropy ratio was found to be consistent with mixing length theory, suggesting a potential closure in the fluid dynamic system.

Unlike the atmosphere of Venus which is completely controlled by the absorbed solar radiation, the outer planets Jupiter and Saturn emit more energy than they receive from the Sun. Like in a star, their optically thick tropospheres must form convection layers where planetary energy from the interior is transported upward. At the same time, solar differential heating is inducing global scale meridional motions which redistribute angular momentum to build up superrotation and differential rotation. Supported by a numerical simulation, we had suggested in Paper I that the realization of this star-earth dualism – emitting energy from the interior while receiving solar energy at low latitudes – may provide the key to our understanding of the mean zonal circulations, in particular the equatorial jets, on Jupiter and Saturn.

The present paper describes a numerical model applicable to Jupiter, and an analytical study is presented elucidating the conditions leading to differential rotation in an atmosphere which is convectively unstable.

Following Paper I, our approach is to consider a linear system forced by solar differential heating. Nonlinear effects arising from advection are represented in the form of eddy diffusion. In Section II of this paper the properties of the model and its limitations are discussed. In Section III an empirical, latitudinal spectrum of the observed zonal wind field on Jupiter is discussed. In Section IV numerical solutions are presented which reveal banded wind fields with alternating and equatorial zonal jets and a multi-cellular Ferrel–Thomson meridional circulation consistent with the observed cloud striations on Jupiter. In Section V the vertical derivatives are parameterized to construct a simplified one-layer model. Such approximation allows us to study the dynamic properties of the atmospheres over a wide range of parameters so that a comprehensive understanding can be obtained.

2. Theoretical Model

We adopt essentially the spectral model formulated in Paper I. Our definitions of the variables are the same and so are the equations to which we refer with the prefix I. Here we summarize the physical and mathematical properties of the model as they apply to Jupiter.

A linear axi-symmetric model is formulated by taking the zonal and time averages on the equations of energy, mass and momentum conservation. Moreover, the following assumptions are made:

(a) Thin layer approximation $1/r \ll \partial/\partial r$,
(b) hydrostatic equilibrium in the vertical direction,
(c) gravity $\gg \omega_p^2 r$,
(d) the large scale flows are characterized by $\bar{U}/r\omega_p \ll 1$,
(e) perturbations on the thermodynamic variables due to solar differential heating are small,
(f) the zonally averaged effects of non-linear advections are represented by down-gradient diffusion (mixing length approximation).

The assumptions (a) through (d) are trivial. However, the assumptions (e) and (f), which are important for our analysis, require justification.

For the atmospheric motions which interest us it is generally justified to assume that the perturbations on the thermodynamic variables are small. In the case of fast rotation (Jupiter and Saturn), the Coriolis force or the meridional advection of *planetary* angular momentum, $\propto \omega_p$, is of major importance. In an atmosphere dominated by the Sun's radiative input and a strong internal planetary source (Jupiter and Saturn), the global scale meridional advection of energy is also of major importance. Both large scale processes can be described in the framework of a linear system. In the *smaller scale*, however, the non-linear effects of energy and angular momentum transfer become important and must be considered. This is extremely difficult, and, to make the problem tractable, simplifications must be made.

Following Williams and Robinson (1973), Durney and Roxburgh (1971) and Rüdiger (1980), we adopt an anisotropic eddy diffusivity to represent the effects of non-linear advections in the smaller scales. Specifically, we write the cross correlation between the velocity vector **V** and an arbitrary quantity E as

$$\overline{\mathbf{V}E} = -\lambda_i V_i \frac{\partial}{\partial x_i} \bar{E}\mathbf{x}_i \equiv -\eta_i \frac{\partial}{\partial x_i} \bar{E}\mathbf{x}_i, \tag{1}$$

where the subscript i indicates a spatial direction, $\mathbf{x}_i$ are the corresponding unit vectors, λ_i and V_i are the mixing length and velocity fluctuations (r.m.s.) in that direction, and their products are combined into a kinematic viscosity η_i. *This is strictly a working hypothesis.*

In a stratified rotating fluid, the motions are affected by rotation, and the eddy diffusion is neither homogeneous nor isotropic. As a working hypothesis we assume that, to first order, the mixing length approximation can absorb these complications. It has yielded interesting results (Williams and Robinson, 1973) and still proves to be useful while we are in this early stage of exploring planetary atmospheres.

By choosing the eddy diffusion to have a form similar to molecular diffusion (Durney and Roxburgh, 1971; Williams and Robinson, 1973) angular momentum is conserved. Furthermore, rigid shell rotation is then a stationary solution in the absence of external forces.

We emphasize that, in the framework of a zonally symmetric circulation and without horizontal eddy diffusion, equatorial motions cannot be maintained (e.g., Hide, 1969; Held and Hou, 1980). This is true for any linear or nonlinear two-dimensional system. With the inclusion of horizontal eddy diffusion such a constraint does not exist (Williams and Robinson, 1973), and the equator can then superrotate or subrotate. The equatorial circulation being an important element of our model, this implies that the invoked horizontal eddy diffusion must in part arise from three dimensional motions. We refer therefore to a *quasi*-axisymmetric circulation.

Ignoring the products of perturbed variables and expanding them in terms of vector spherical harmonics (I1 through I3), the linearized equations of energy, mass and momentum conservation are presented in Paper I (I4 through I8). For the outer planets where $\omega_A \ll \omega_p$, it is justified to assume $\omega_1 \sim \omega_2 \sim \omega_p$.

In our model, the circulation is driven by solar differential heating, and we consider only the lowest order symmetric component q_2 where most of the energy is deposited (e.g., Volland and Mayr, 1972a). This assumption (I12 and I13) is not required for the calculations, but serves to simplify the discussion.

No separable eigenfunctions exist to describe the latitude dependence in a quasi-zonally symmetric circulation where global scale momentum advection (Coriolis force) and eddy diffusion are important (Chapman and Lindzen, 1970; Volland and Mayr, 1972b). In our model, spherical harmonics merely serve as basis functions. The variables on the left hand sides of Equations I4 through I8 and the associated spherical harmonics P_ℓ, $\mathbf{B}_\ell$, $\mathbf{C}_{\ell-1}$ are viewed as 'modes' with wave number ℓ. The terms on the right hand sides of I7 and I8 can then be viewed to represent mode coupling which arises from the Coriolis force and involves the field quantities of adjacent modes (Figure 1).

The lowest order mode ($\ell = 2$) describes the rigid shell component of superrotation. In this mode, the atmospheric angular velocity is associated with the solenoidal vector spherical harmonic C_1 and is independent of latitude. Only this component has a non-vanishing net global angular momentum at a fixed altitude level, and it was shown in Paper I how the atmosphere can receive this angular momentum from the planet (or planetary interior) during spin up. The higher order modes ($\ell \geqslant 4$) describe differential rotation and their contributions to the net global angular momentum are identically zero.

3. Empirical Spectrum

Figure 2 shows an empirical representation of the Voyager data (Smith *et al.*, 1979b) in terms of vector spherical harmonics. The amplitudes in the lower part of Figure 2 represent the coefficients of solenoidal harmonics $\mathbf{C}_{\ell-1}$ (Morse and Feschbach, 1953) with the sign convention that the positive and negative values contribute to superrotation (positive zonal velocities) and subrotation (negative velocities) at the equator respectively. In the upper part of Figure 2, empirical representations of the Voyager I data (from both hemispheres) are presented for syntheses up to order $\ell \leqslant 12$ and 34. Included are only the harmonics which are symmetrical with respect to the equator (even wave numbers ℓ).

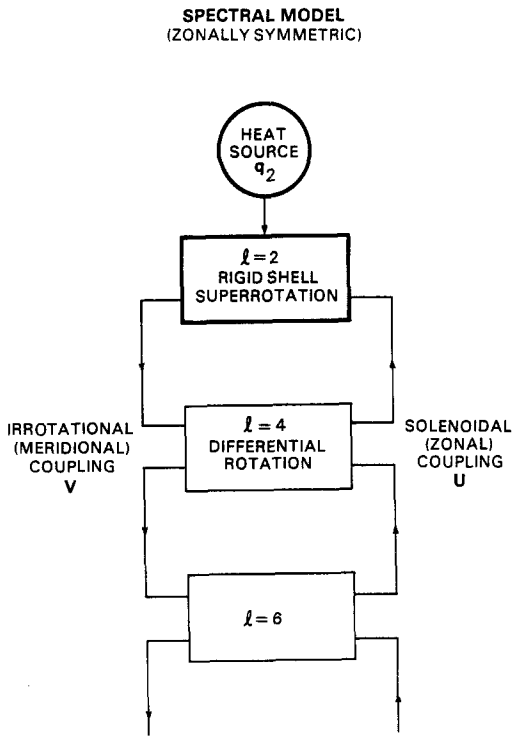

Fig. 1. Block diagram illustrating the mode/Coriolis coupling in the spectral model. The heat source in the fundamental mode, q_2, is directly forcing the rigid shell component (or global average) of superrotation. Coriolis coupling through the irrotational (meridional) velocity field (which is curl free) is driving differential rotation by cascading momentum from lower to higher order modes (left hand side of the chain link). The feed back through the solenoidal (zonal) velocity field (which is divergence free) is capable of trapping energy and angular momentum in the lower order modes.

The fundamental harmonic ($\ell = 2$) or the rigid shell component of superrotation dominates. Higher order modes, $\ell \geqslant 4$, are at least a factor of two smaller and apparently in a separate class of their own. After the abrupt decrease between $\ell = 2$ and $\ell = 4$, the amplitudes decrease gradually and monotonically toward higher wave numbers and, up to $\ell = 18$, contribute to equatorial superrotation. Then the sign changes, and the spectrum up to $\ell = 28$ contributes to equatorial subrotation. The spectra for the Voyager I and II observations are nearly identical.

Anticipating the theoretical results later on discussed, we offer the following interpretation. The dominant rigid shell component of superrotation ($\ell = 2$) is primarily driven by solar differential heating where most of the energy is deposited in the lowest order mode. In contrast, the solar input into the higher order modes is relatively small. This part of the spectrum (representing differential rotation), however, can be excited by mode coupling where momentum and energy effectively cascade from lower to higher order modes.

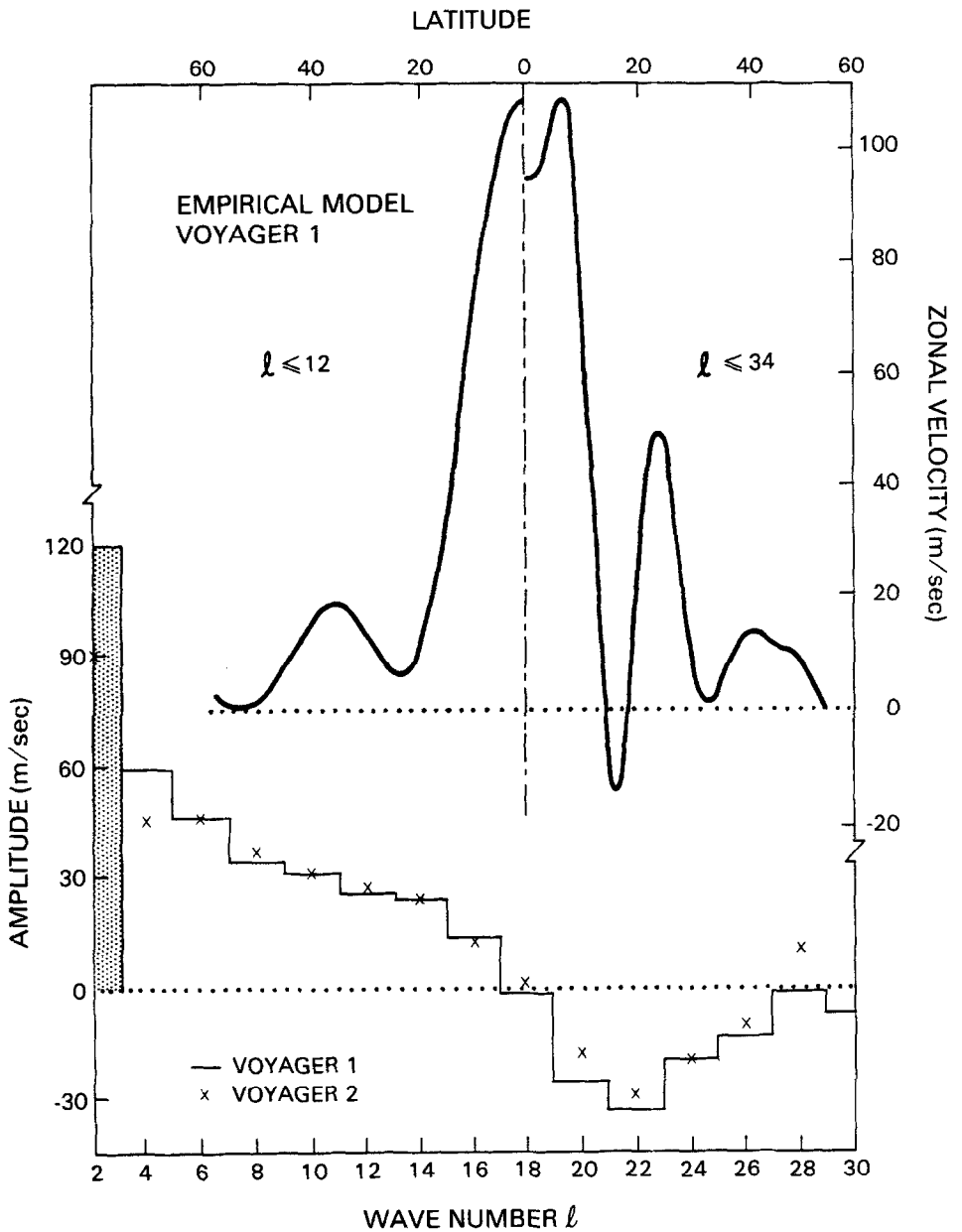

Fig. 2. Empirical model of the zonal wind velocities observed from the Voyager spacecraft (Smith *et al.*, 1979b) in terms of the solenoidal (divergence free) vector spherical harmonics which are used as basis functions in the theoretical model. Data from both hemispheres are taken, but only the components symmetrical with respect to the equator are presented in the lower part of the figure. Syntheses up to wave numbers $\ell = 12$ (left) and 34 (right) are shown in the upper part. The rigid shell component ($\ell = 2$) directly driven by solar differential heating (q_2) dominates. The higher order components ($\ell > 2$) describing differential rotation are smaller by at least a factor of two and are apparently in a separate class of their own. Note the alternating pattern in the power spectrum and that the Voyager I and II spectra are nearly identical.

4. Numerical Results

In Paper I, the heat flux due to eddy diffusion was formulated in terms of the kinetic temperature (Equation I4). More appropriately, the heat flux has the general form (e.g. Chan *et al.*, 1982)

$$J_i = -\rho\kappa_i\left(\frac{\partial T}{\partial x_i} - \frac{(\gamma-1)}{\gamma}\frac{T}{p}\frac{\partial p}{\partial x_i}\right), \tag{2}$$

where γ is the ratio between the specific heats at constant pressure and volume (for a diatomic gas, $(\gamma-1)/\gamma = 2/7$). The expression in the paranthesis of Equation (2) represents the gradient of the potential temperature. Applying linear perturbation theory and assuming hydrostatic equilibrium, the pressure term in Equation (2) vanishes in the vertical direction $\Delta[(T/p)(\partial p/\partial r)] = 0$ (see Equation I6). In the horizontal direction, the heat flux is affected by the pressue gradient, but its contribution is generally small compared to that from the temperature gradient. For completeness, this term is now included in our numerical analysis.

With homogeneous boundary conditions and a heat source of the form (I12) and (I13), the (modified) energy, continuity and momentum equations (I4–I8) are solved for a limited number of 20 symmetric (even) modes from $\ell = 2$ to 40. Since mode coupling is considered in self-consistent form, this requires a large system of 100 ordinary first and second order differential equations to be integrated in altitude. The system is in blocked tridiagonal form, for which there exist reliable solution procedures. With a vertical step size of 5 km, the altitude range is limited between the 25 and the 5×10^{-5} bar pressure levels. We note that this depth may not be totally adequate to describe the Jovian circulation. Corresponding to the largest wave number $\ell = 40$, the shortest horizontal wave length is 9°, which cannot provide sufficient resolution to describe the observed details in the Jovian circulation. These limitations in the dimensions of the model are dictated by the computer.

As input, a global average atmosphere is adopted which rotates at a rate of 1.8×10^{-4} in a gravitational field with $g = 2400\,\mathrm{cm\,s^{-2}}$, representative of the conditions on Jupiter. The temperature distribution shown in Figure 3 is based on the infrared measurements from the Voyager spacecrafts (Hanel *et al.*, 1979a, b). Above the 2 mb level we assume the temperature to be constant.

For the energy source driving the circulation, $q_2(r)$, we chose a height distribution shown in Figure 3 which we adopt from the work of Wallace *et al.* (1974). The heat input increases with height and produces the temperature inversion above the tropopause. Radiative cooling is considered in the form of a Newtonian coefficient $\alpha = p_0\alpha_\infty\,(1 - \exp(-3 \times 10^5/p_0)^4)$ (ergs deg^{-1} s^{-1} gm^{-1}), where $\alpha_\infty = 6.5 \times 10^{-6}$ is provided by B. J. Conrath (private communication). The exponential term is adopted to simulate the trapping of radiation in the lower troposphere.

In the troposphere of Jupiter where energy must be convected out of the hot planetary interior, the temperature lapse rate should be weakly superadiabatic. The characteristic latitudinal structure of the circulation depends on the stability $S_0 \equiv (\partial T_0/\partial r) + \Gamma$,

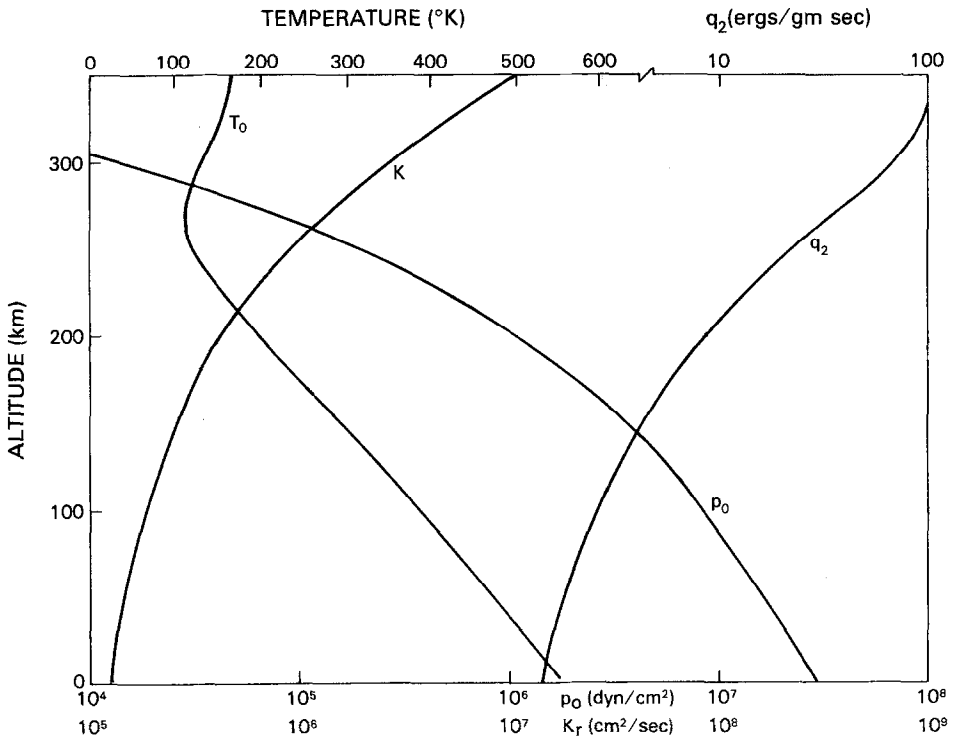

Fig. 3. Input data for the average temperature, T_0, pressure, p_0, and the heat source, q_2. Above the 1 mb pressure level the temperature is assumed to be constant. In the troposphere, a negative stability $S_0 = -1.7 \times 10^{-6}\,\mathrm{K\,cm^{-1}}$ is adopted which is small (10%) compared to the adiabatic lapse rate, $\Gamma = 1.7 \times 10^{-5}$. With a relative mixing factor $K_\theta/K_r \simeq 5 \times 10^4$ (consistent with mixing length theory), the vertical eddy diffusion coefficient is $K_r = 1.2 \times 10^5$ at the lower boundary (25 bar pressure) and is assumed to increase with height at a rate inversely proportional to the square root of the density. The Prandtl number is assumed to be one.

where $\Gamma = 1.7 \times 10^{-5}\,(\mathrm{K\,cm^{-1}})$ is the adiabatic lapse rate. Based on observations, it was estimated (Paper I) that the stability of the upper troposphere should be on the order of -10^{-6}. For our numerical model, whose latitudinal resolution is limited, we chose a value of $S_0 = -1.7 \times 10^{-6}$ which is 10% of the adiabatic lapse rate. The stability is forced to approach zero near the lower boundary. It will be shown later on that the computed circulation depends rather sensitively on S_0.

Since radiative cooling is much less important than eddy heat conduction in the optically thick troposphere, the magnitudes of the temperature variations and zonal velocities (not the vertical and meridional components) vary proportional to the solar heat input and inversely proportional to the eddy diffusion $\propto \Delta q/K$. As can be seen from I4 through I8, the necessary condition is that the circulation is quasi-geostrophic, which requires that the viscous terms in I7 are negligible. This is generally true for the adopted transport coefficients.

Using the heat source shown in Figure 3, the eddy diffusion coefficients are chosen to reproduce the observed magnitudes in the zonal velocities. Thus, the vertical coefficient is taken to be $K_r = 1.2 \times 10^5 (\mathrm{cm^2\,s^{-1}})$ at the lower boundary and is assumed to increase with height at a rate inversely proportional to the square root of the density (Chapman and Lindzen, 1970). The Prandtl number is assumed to be one.

With a temperature $T_0 = 170\,\mathrm{K}$ and given the adopted stability and vertical eddy diffusion coefficient $K_r = 3 \times 10^5$ at the one bar pressure level, the average upward flux of energy

$$F = -c_p \rho_0 K_r S_0 = -\frac{7}{2}\frac{p_0}{T_0} K_r S_0 \tag{3}$$

is about $10^{-4}\,\mathrm{ergs\,cm^{-2}\,s^{-1}}$, which is in reasonable agreement with the observations (Orton and Ingersoll, 1976). Noting that the vertical velocities W (not shown) are on the order of $3 \times 10^{-2}\,\mathrm{cm\,s^{-1}}$, the above eddy diffusion coefficient is also of the right order of magnitude to be consistent with mixing length theory ($K_r \sim WH \sim 1.5 \times 10^5\,\mathrm{cm^2\,s^{-1}}$ where H, the density scale height, is about 50 km).

Later on, it will be shown that it is important to adopt a ratio between the horizontal and vertical eddy diffusion coefficients (relative mixing factor) of order $R = 5 \times 10^4$. If this ratio were much larger, the meridional circulation could not maintain a large degree of differential rotation; if it were much smaller, the equator would tend to corotate. With this ratio the horizontal and vertical viscous stresses are of comparable magnitudes. Moreover, this ratio is consistent with mixing length theory which requires $R \sim \mathrm{O}\,(V\lambda_\theta / W\lambda_r) \sim \mathrm{O}\,(\lambda_\theta^2/\lambda_r^2)$, where λ_θ and λ_r are the characteristic horizontal (in latitude) and vertical dimensions of the mean meridional circulation respectively.

In Figure 4 the results are shown for the temperature amplitude and the meridional and zonal velocities at 75, 200, and 400 km. The altitude scale is defined relative to the lower boundary; the tropopause being near 250 km (see Figure 3). Also shown are the power spectra for the zonal velocity. In the troposphere (75 and 200 km, with $S_0 < 0$), the results reveal a number of features which have some resemblance to Jupiter. The equatorial jet and the banded wind field are reproduced. More specficially, the computed power spectra show characteristics similar to those inferred from observations (Figure 2). The fundamental component or the rigid shell component of superrotation ($\ell = 2$), directly driven by solar differential heating, dominates. Distinct from that, the higher order modes induced by mode (Coriolis) coupling are in a separate class and reveal an alternating pattern in ℓ space, in substantial agreement with the data (Figure 2). The meridional velocity field indicates a number of cells. The computed temperature distribution reveals plateaus similar to those observed by Hanel *et al.* (1979b), but the magnitudes of the perturbations are larger (by about a factor of three) than those observed. Considering the heuristic nature of our model – with the simplifying assumptions about radiative cooling, eddy diffusion and Prandtl number, with the limitations on depth, and the uncertainties on the solar driving – this discrepancy is probably not significant.

At higher altitudes (400 km), in the stratosphere which is convectively stable, the

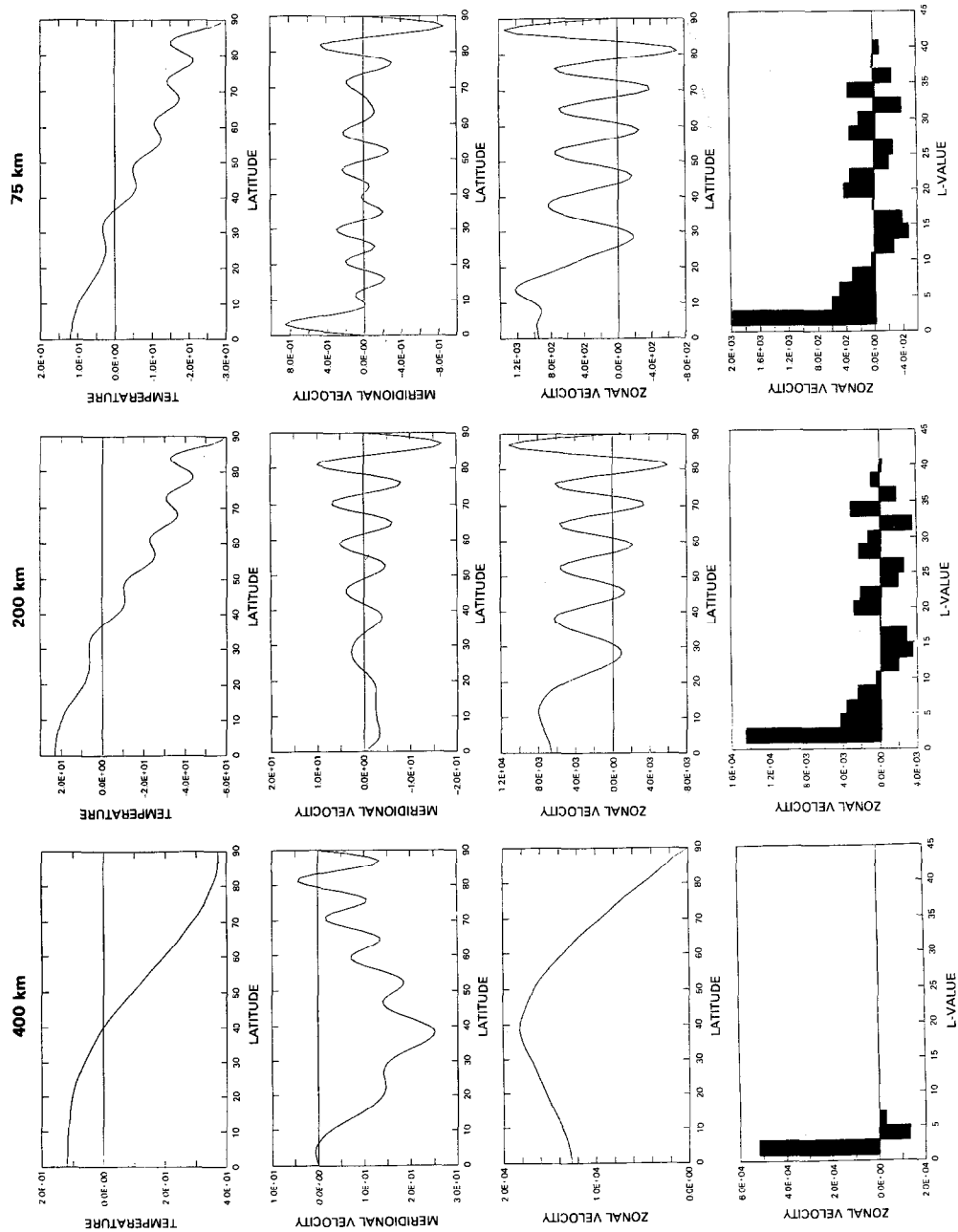

Fig. 4. The computed latitudinal variations in the temperature and the meridional and zonal velocities at a few selected altitudes. Also shown are the power spectra for the zonal velocities. Note the zonal wind bands and equatorial jets in the troposphere (the tropopause is at an altitude near 250 km), resembling the velocity field of Jupiter. In the stratosphere at higher altitudes a broad velocity jet develops at mid latitudes.

results are entirely different. Bands no longer form in the velocity field and there is no equatorial jet. Instead, a broad maximum develops in the zonal velocity at mid-latitudes, and the meridional component is almost uniformly directed toward the pole. Concomittantly, the power spectrum is also different. The fundamental rigid shell component is still positive (superrotation) since it is directly driven by solar radiation; but the higher order modes are negative, small and rapidly decay toward higher wave numbers. Moreover, the temperature amplitude reveals a broad plateau at equatorial latitudes. Qualitatively, these features are similar to those observed in the stratosphere of Venus (e.g., Schubert *et al.*, 1980) and agree with the conclusions of Paper I.

The meridional velocity field has the form of a multicellular Ferrel-Thompson circulation similar to that shown in Paper I (Figure 8), except that the present model, with its higher resolution, shows eleven cells in the troposphere. Considering the number of observed narrow bands in the cloud cover of Jupiter, this result is probably more realistic.

Computer experiments show that, at tropospheric altitudes, relatively small changes in S_0, on the order of a few percent, can have profound effects on the velocity and temperature fields. This dependence on the stability requires us to look more closely at the characteristics of the linear system. Thus, to facilitate our investigation over a wide range of parameters, a single-layer model is formulated which permits us also to include a very large number of horizontal modes with virtually unlimited latitudinal resolution. While providing the necessary insight, this model produces results similar to those discussed in Figure 4.

5. One-Layer Model

For completeness, we start with a set of equations which is almost identical to that in the discussion section of Paper I.

$$-\frac{1}{\rho_0}\frac{\partial}{\partial r}\kappa_r\rho_0\frac{\partial \Delta T_\ell}{\partial r} = \frac{\kappa_r}{h^2}\Delta T_\ell, \tag{4}$$

$$-\frac{1}{\rho_0}\frac{\partial}{\partial r}\eta_r\rho_0\frac{\partial U_{\ell-1}}{\partial r} = \frac{\eta_r}{h^2}U_{\ell-1}, \tag{5}$$

$$-\frac{1}{\rho_0}\frac{\partial}{\partial r}\eta_r\rho_0\frac{\partial V_\ell}{\partial r} = \frac{\eta_r}{h^2}V_\ell, \tag{6}$$

$$\Delta \log p_\ell = \frac{dmg}{kT_0^2}\Delta T_\ell, \tag{7}$$

$$W_\ell = -\sqrt{\ell(\ell+1)}\frac{d}{r}V_\ell; \tag{8}$$

where h and d, defined later, are scale-lengths of the order of the density scale-height.

Substitution of (4)–(8) into (I4)–(I8) yields

$$\left(\frac{\alpha P}{c_p}+\frac{\ell(\ell+1)}{r^2}K_\theta+\frac{K_r}{h^2}\right)\frac{\Delta T_\ell}{P}-\sqrt{\ell(\ell+1)}\,\frac{d}{r}S_0V_\ell=\frac{q_\ell}{c_p}, \tag{9}$$

$$\sqrt{\ell(\ell+1)}\,g\frac{d}{r}\frac{\Delta T_\ell}{T_0}-\Omega(U_{\ell-1}-U_{\ell+1})+\left[\left(\frac{4}{3}\frac{\ell(\ell+1)-2}{r^2}K_\theta+\frac{K_r}{h^2}\right)V_\ell\right]=0, \tag{10}$$

$$\left(\frac{\ell(\ell-1)-2}{r^2}K_\theta+\frac{K_r}{h^2}\right)U_{\ell-1}-\Omega(V_{\ell-2}-V_\ell)=0, \tag{11}$$

with

$$\kappa=\frac{c_pK}{P}, \qquad \eta=K, \tag{12}$$

where, omitting subscripts, K is the eddy diffusion coefficient, and Ω is approximately the rotation rate of the atmosphere ($\Omega\sim\omega_p$ for Jupiter).

Equations (9) and (11) describe the conservation of energy and angular momentum respectively. Except for the diffusion term in square brackets, Equation (10) represents the thermal wind relationship describing the coupling between energy and angular momentum.

5.1. ANALYSIS

In matrix form, the above set of equations can be written as

$$A_\ell\Delta_\ell=Q_\ell+C^-\Delta_{\ell-2}+C^+\Delta_{\ell+2}, \tag{13}$$

where

$$\Delta_\ell=\begin{Bmatrix}\Delta T_\ell\\ U_{\ell-1}\\ V_\ell\end{Bmatrix},\quad \Delta_{\ell-2}=\begin{Bmatrix}\Delta T_{\ell-2}\\ U_{\ell-3}\\ V_{\ell-2}\end{Bmatrix},\quad \Delta_{\ell+2}=\begin{Bmatrix}\Delta T_{\ell+2}\\ U_{\ell+1}\\ V_{\ell+2}\end{Bmatrix};$$

$$Q_\ell=\begin{Bmatrix}q_\ell/c_p\\ 0\\ 0\end{Bmatrix},$$

$$A_\ell=\begin{Bmatrix}a_\ell & 0 & -b_\ell\\ c_\ell & -\Omega & d_\ell\\ 0 & e_\ell & \Omega\end{Bmatrix},$$

$$C^-=\begin{Bmatrix}0&0&0\\0&0&0\\0&0&\Omega\end{Bmatrix},$$

$$C^+=\begin{Bmatrix}0&0&0\\0&-\Omega&0\\0&0&0\end{Bmatrix}, \tag{14}$$

and

$$
\begin{aligned}
a_\ell &= \left(\frac{\alpha P}{c_p} + \frac{\ell(\ell+1)}{r^2} K_\theta + \frac{K_r}{h^2}\right)\frac{1}{P}, \\
b_\ell &= \sqrt{\ell(\ell+1)}\,\frac{d}{r} S_0, \\
c_\ell &= \sqrt{\ell(\ell+1)}\,\frac{g}{T_0}\frac{d}{r}, \\
d_\ell &= \frac{4}{3}\frac{\ell(\ell+1)-2}{r^2} K_\theta + \frac{K_r}{h^2}, \\
e_\ell &= \frac{\ell(\ell-1)-2}{r^2} K_\theta + \frac{K_r}{h^2}.
\end{aligned}
\tag{15}
$$

Equation (13) states in concise form that a particular harmonic mode $\Delta_\ell = (\Delta T_\ell, U_{\ell-1}, V_\ell)$ can be excited directly through the heat source Q_ℓ or indirectly through Coriolis coupling (C^+, C^-) involving the adjacent modes (see also Figure 1). The solution of this set of equations can be interpreted as a boundary value problem in ℓ space. At the outer boundary the zonal velocity $U_{\ell+1}$ is assumed to be negligible; at the inner boundary, $V_0 = 0$.

In general, the feed back from the higher order modes $\Delta_{\ell+2} = (\Delta T_{\ell+2}, U_{\ell+1}, V_{\ell+2})$ due to Coriolis coupling is important and requires the simultaneous solution of Equation (13) for a sufficiently large number of modes. It is verified through computer experiments that convergence in the power spectrum can always be assured. At higher wave numbers the potential for transferring energy and momentum through global scale advection (Coriolis force) is eventually exhausted, and horizontal eddy diffusion (small scale advection) becomes progressively more important in damping the amplitudes.

If we ignore the higher order mode $\Delta_{\ell+2}$ in Equation (13), the asymptotic behavior of Δ_ℓ for large ℓ can be estimated as

$$
\Delta_\ell = \frac{1}{M_\ell + D_\ell + 1}\begin{Bmatrix} 0 & 0 & b_\ell/a_\ell \\ 0 & 0 & (a_\ell d_\ell + b_\ell c_\ell)/a_\ell \Omega \\ 0 & 0 & 1 \end{Bmatrix} \Delta_{\ell-2}, \tag{16}
$$

where

$$
M_\ell \equiv \frac{e_\ell b_\ell c_\ell}{a_\ell \Omega^2} = \frac{S_0 \ell(\ell+1) g d^2}{T_0 \Omega^2 r^2} P_\alpha \tag{17}
$$

and

$$
D_\ell \equiv \frac{d_\ell e_\ell}{\Omega^2} = \frac{\left(\frac{4}{3}\frac{\ell(\ell+1)-2}{r^2} K_\theta + \frac{K_r}{h^2}\right)\left(\frac{\ell(\ell-1)-2}{r^2} K_\theta + \frac{K_r}{h^2}\right)}{\Omega^2} \tag{18}
$$

In Equation (17) a 'radiative Prandtl number'

$$P_\alpha \equiv \frac{P\left(\frac{\ell(\ell-1)-2}{r^2}K_\theta + \frac{K_r}{h^2}\right)}{\frac{\alpha P}{c_p} + \frac{\ell(\ell+1)}{r^2}K_\theta + \frac{K_r}{h^2}} \tag{19}$$

is introduced which has the properties $P_\alpha \to O(P) \sim P$ (for small α) and $P_\alpha \to 0$ (for large α). The denominator $M_\ell + D_\ell + 1$ of Eqution (16) comes from the determinant of A_ℓ. The magnitudes of the dimensionless parameters M_ℓ and D_ℓ tend to increase proportional to ℓ^2 and ℓ^4 respectively.

We define a 'characteristic wave number' L such that

$$|M_L| + D_L = 1. \tag{20}$$

Unlike the integer ℓ which is an independent variable, L is a continuous function of the atmospheric parameters and therefore *not necessarily an integer number*. In the regime of large wave numbers, $\ell > L$, the magnitude of the denominator in (16) increases above one, causing the amplitudes of the power spectrum to decay very rapidly. The assumption $\Delta_{\ell+2} \ll \Delta_\ell$ for Equation (16) is then justified.

D_L is positive definite and has the form of an Ekman number squared. Under most circumstances, $D_L \ll 1$. Considering that the parameter is proportional to the square bracket in (10), this is equivalent to the assumption of geostrophy which is closely satisfied for the numerical results discussed in Section 4. We shall focus on this regime in the subsequent study. Some characteristics of the ageostrophic flow will be briefly discussed later on.

5.2. GEOSTROPHIC FLOW

In the geostrophic regime,

$$M_\Omega = \frac{S_0 g d^2 P_\alpha}{T_0 r^2 \Omega^2} \tag{21}$$

is the crucial parameter determining the nature and the horizontal structure of the circulation. The characteristic wave number defined in (20) is approximately given by

$$L \sim \sqrt{L(L+1)} \sim |M_\Omega|^{-1/2} = \frac{r\Omega}{d}\sqrt{\frac{T_0}{|S_0|gP_\alpha}}; \tag{22}$$

and, analogous to Equation (I30), one can then estimate the characteristic latitudinal scale of the circulation, $\Delta\theta = 360°/L$. In the vase of Venus, the parameter $M_\Omega > 1$. Thus, the feedback from the higher order modes $\Delta_{\ell+2}$ [last term on the right hand side of Equation (13)] is always negligible, and an approximate solution can be obtained through recursion (I23 through I26).

If we assume that $P_\alpha = 1$ and with a reasonable negative stability ($S_0 < 0$) for the troposphere of Jupiter, it follows that $M_\Omega < 0$ with $|M_\Omega| \ll 1$. Thus the denominator in Equation (16) is nearly constant for $\ell < L$, and the power spectra of the solution

amplitudes Δ_ℓ do not converge rapidly. A closed or recursive solution does not exist, and Coriolis coupling must be considered in self-consistent form. For $\ell \sim L$, the denominator $[M_\ell + (D_\ell) + 1]$ in (16) becomes very small and a 'near resonance' condition can develop. Large amplitudes are then excited in modes of order L which are not *directly* driven by the heat source q_2. Since all the modes are coupled (see Figure 1 and Equation (13)), this resonance affects the entire power spectrum, least of all the fundamental mode Δ_2 which is to a large extent forced by q_2; thus, the resonance will primarily affect differential rotation. In our model, this is the basic mechanism for driving the banded wind field of Jupiter.

In the following, we shall present numerical solutions of the Equations (9) through (11) (or Equation (13)) to illustrate some important properties of a rotating atmosphere. We neglect radiative cooling and assume $P_\alpha \sim P = 1$. The adopted input parameters are $T_0 = 170\,\mathrm{K}$, $h = 50\,\mathrm{km}$, $d = 100\,\mathrm{km}$ and $q_2 = 15\,\mathrm{ergs\,gm^{-1}\,s^{-1}}$. The other parameters, planetary rotation rate, radius and gravitational acceleration, have the standard values for Jupiter. For the vertical and horizontal eddy diffusion coefficients the values 10^5 and 5×10^9 are chosen, well within the geostrophic regime ($D_L \ll 1$). To assure convergence, a large number of modes are considered. The cut-off is chosen at a wave number of about $5L$ [with L defined in Equation (20)] which may be as large as 200.

On a globe with finite dimension, the above discussed resonance has a discrete nature. In the framework of our spectral model, for a given stability, M_ℓ does not vary continuously but in steps with the discrete values of ℓ. Conversely, there are discrete values of stability for which the resonance condition is more or less satisfied. To illustrate this point, a parametric study is presented. For 2000 values of stability in the range from $S_0 = -10^{-5}$ to -10^{-7}, solutions of Equation (13) are obtained. For each solution, the zonal velocity component C_3 ($\ell = 4$) is presented in Figure 5 as a function of the characteristic wave number $L = L(S_0)$. The relationship between L and S_0 from Equation (20) is shown in a separate panel. In the range of L from 20 to 30, for example, 6 different resonances appear. This is somewhat larger than the 5 resonances associated with all the even wave numbers in the interval which would develop if the denominator in (16) were the only controlling factor. Since Equation (16) is an analytical estimate which also depends on the solution vector $\Delta_{\ell-2}$, one can readily see why $M_L + (D_L) + 1 = 0$ is not the precise condition for a resonance.

In the vicinity of a resonance, the velocity components are large. Relatively small changes in the stability can then be very effective in changing the differential rotation. Moreover, Figure 5 shows that two resonance branches are excited: one with a positive velocity and the other one with a negative velocity. This can be readily understood considering that, for negative S_0, the smallest value $M_\ell + (D_\ell) + 1$ ($\ell = 2, 4, \ldots$) in Equation (16) can be either positive or negative.

For comparison we also show in a separate panel the results obtained with positive stabilities ranging from $S_0 = 10^{-7}$ to 10^{-5}. Here the velocity amplitude, as a function of the characteristic wave number L, varies monotonically and no resonance develops.

Adopting a stability of -10^{-6}, a complete solution is shown in Figure 6 for the

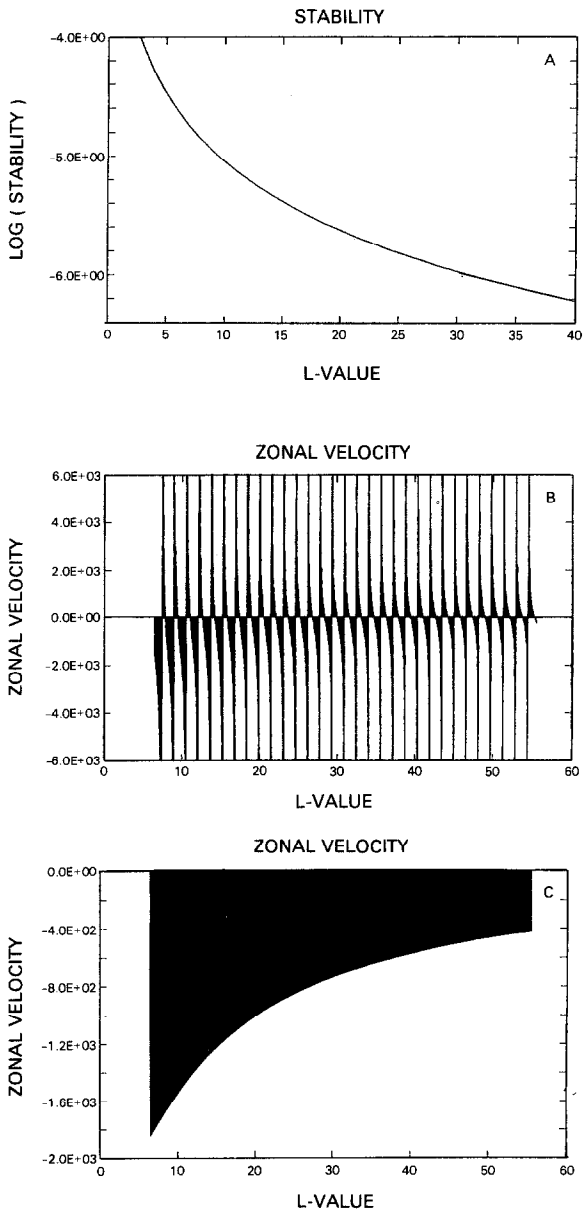

Fig. 5. Solutions of the simplified equation (13) are obtained to study the sensitivity over a wide range of negative and positive stabilities ranging in magnitude from -10^{-7} to -10^{-5} K cm^{-1}. Panel *A* shows the relationship between $|S_0|$ and the characteristic wave number L which is defined in (20). Unlike the integer wave number ℓ, L *is* a continuous function of $|S_0|$ and therefor *not an integer number.* In panel *B* we show the first component in the power spectrum of differential rotation, C_3 (which is not directly driven by the solar heat input q_2), plotted against L. For negative stability ($S_0 < 0$), discrete resonances develop. In contrast, the functional dependence between C_3 and S_0 is continuous in panel *C* where the stability is assumed to be positive ($S_0 > 0$).

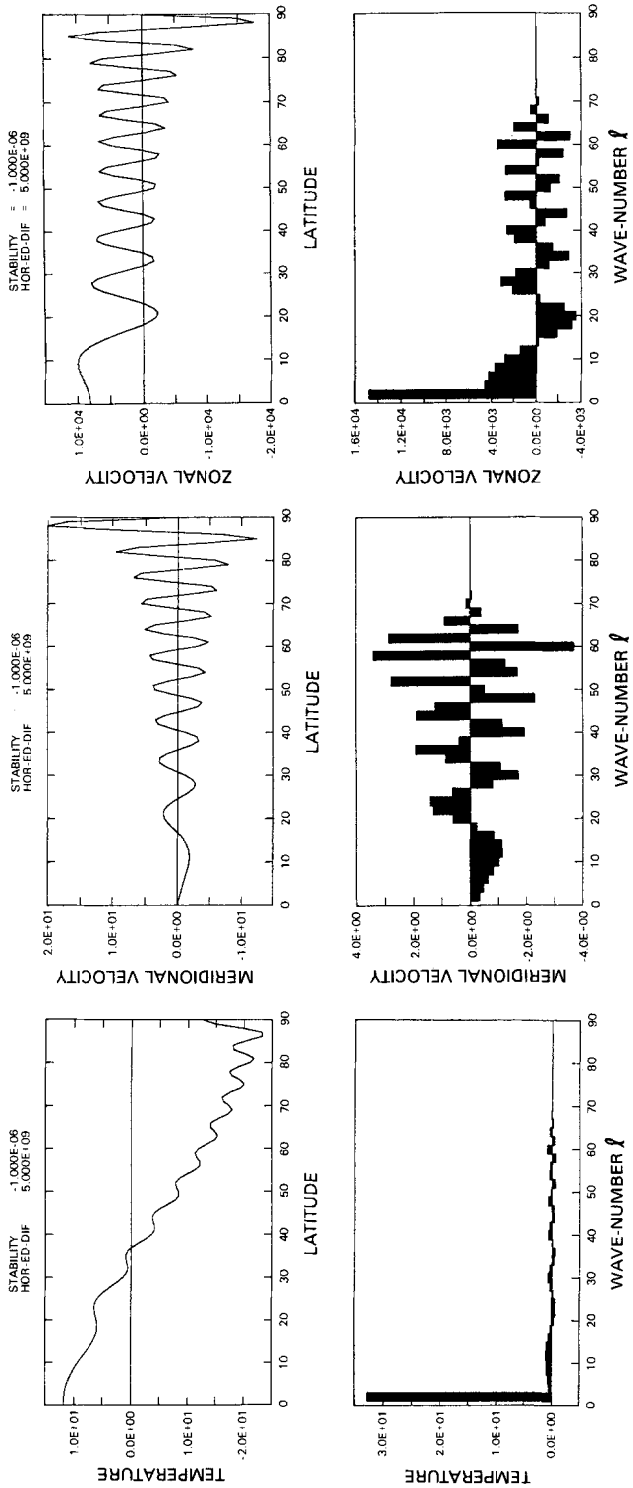

Fig. 6. For $S_0 = -10^{-6}$ K cm^{-1}, $T_0 = 170$ K, $H = 50$ km, $d = 100$ km, $K_r = 10^5$, and $K_\theta = 5 \times 10^9$, a solution of Equation (13) is presented which is in the positive branch near a resonance. Note that the number of zonal jets (including the equatorial one) is consistent with the observations in the Jovian circulation.

temperature, and the meridional and zonal velocities. The adopted stability reproduces the number of zonal jets which are observed on Jupiter below 60° latitude. Consistent with the infrared measurements on Voyager (Hanel *et al.*, 1979a, b), the temperature reveals variations on the order of 10 K. For a given zonal velocity, the temperature contrast decreases with increasing depth of the atmosphere which is chosen to be 1000 km. Consistent with the banded structure of the zonal velocity, the meridional velocity field (its upper branch) is multicellular. The results closely resemble those from the numerical integration at lower altitudes in Figure 4.

Also shown in Figure 6 are the power spectra. The cut-off wave number is 150. We see that the amplitudes begin to decrease rapidly above $\ell = 62$ and can no longer be discerned at a wave number of 80. The power spectrum clearly converges. Tests confirm that an extension of the cut-off value does not affect the solution. These results illustrate the problem one faces in describing the Jovian circulation. For realistically small values of stability, one must consider a very large number of modes or a correspondingly small grid size. With limited computer resources, such considerations have essentially dictated our selection of the model parameters (i.e., stability and wave number domain) for the numerical integration earlier presented (Figure 4); and still we cannot be confident that, to some extent, the solution is not affected by truncation.

True resonances of course cannot develop. Regulatory non-linear feed back processes would ultimately prevent that. Moreover, for each singularity there are two resonance branches approaching $\pm\infty$, which represent non-trival solutions of the homogeneous equations [Equation (13), with $Q_\ell = 0$] with the determinant of the entire system set to zero. These two branches have opposite signs, lie infinitely close together in the parameter space and tend to cancel each other. Therefore, only a 'near resonance' can be excited, and, for realistic considerations, its width is of critical importance.

As emphasized before, the resonance affects primarily differential rotation. The degree of differential rotation relative to rigid shell rotation is determined by the relative mixing factor R (the ratio between the horizontal and vertical eddy diffusion coefficients). Adhering to the format of Figure 5, we show in Figure 7 three families of the velocity component C_3 ($\ell = 4$), each belonging to a particular resonance near $L \sim 30$ (indicated with arrows). Specifically, with varying stabilities [or L from Equation (20)] for each family, 500 solutions of Equation (13) are obtained, and, out of velocity spectra of the kind shown in Figure 6, the second harmonic ($\ell = 4$) is presented covering the positive and negative branch of the resonance. For a fixed vertical eddy diffusion coefficient $K_r = 10^5$, three values of horizontal eddy diffusion coefficients are chosen, $K_\theta = 10^9$, 10^{10}, and 10^{11}, corresponding to $R = 10^4$, 10^5, and 10^6 respectively. The results show that the areas spanned by the width of the resonances shrink as the mixing factor and the horizontal eddy diffusion coefficient increase. In the range $R < 10^3$, the velocity spectrum is virtually invariant.

The physical significance of this result is illustrated in Figure 8. Here, a computer experiment is presented where we vary from left to right the mixing factor or horizontal eddy diffusion coefficient K_θ which is again 10^9, 10^{10}, and 10^{11} (with $K_r = 10^5$). Three

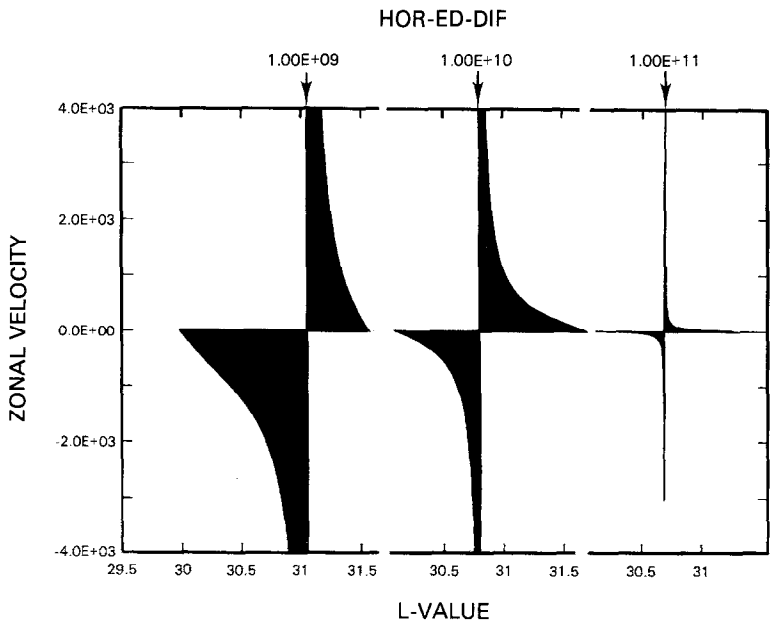

Fig. 7. With the format from Figure 5, we show three different families of the C_3 velocity component in the vicinity of resonances (indicated by arrows) near $L = 30$. The families are computed for relative mixing factors of $R = 10^4$, 10^5, and 10^6. Note that with increasing R the resonance becomes narrower. For $R < 10^3$, where vertical diffusion completely dominates over horizontal diffusion, the velocity field no longer depends on R.

series of velocity fields are computed (from Equation (13)) by slowly varying the stability from $S_0 = -1.07 \times 10^{-6}$ (top) to -9.9×10^{-7} (bottom). The chosen values roughly trace the resonance families shown in Figure 7 (note that according to Equation (20), $L \propto (|S_0|)^{-1/2}$). For the small mixing factor $R = 10^4$ on the left, differential rotation virtually dominates. As the stability slowly changes, the velocity field changes significantly. But the total number of positive jets (10) in the entire latitude range is invariant. Between $S_0 = -9.9 \times 10^{-7}$ and -1.01×10^{-6} (not shown), a resonance occurs and the velocities are much larger. The former stability is in the positive branch, the latter is in the negative branch, and the two velocity fields are completely different. At high latitudes, the zonal jets are out of phase and of comparable magnitude, while at lower latitudes the differences are not that extreme.

For the large mixing factor on the right, $R = 10^6$, rigid shell super-rotation clearly dominates. There is, however, some differential rotation, and the number of positive jets, although they are weak, is again 10. Between $S_0 = -1.01 \times 10^{-6}$ and -1.03×10^{-6} a resonance occurs, but it is so narrow (Figure 7) that the effect on differential rotation is barely visible.

For the intermediate mixing factor, $R = 10^5$, rigid shell superrotation and differential rotation are of comparable importance.

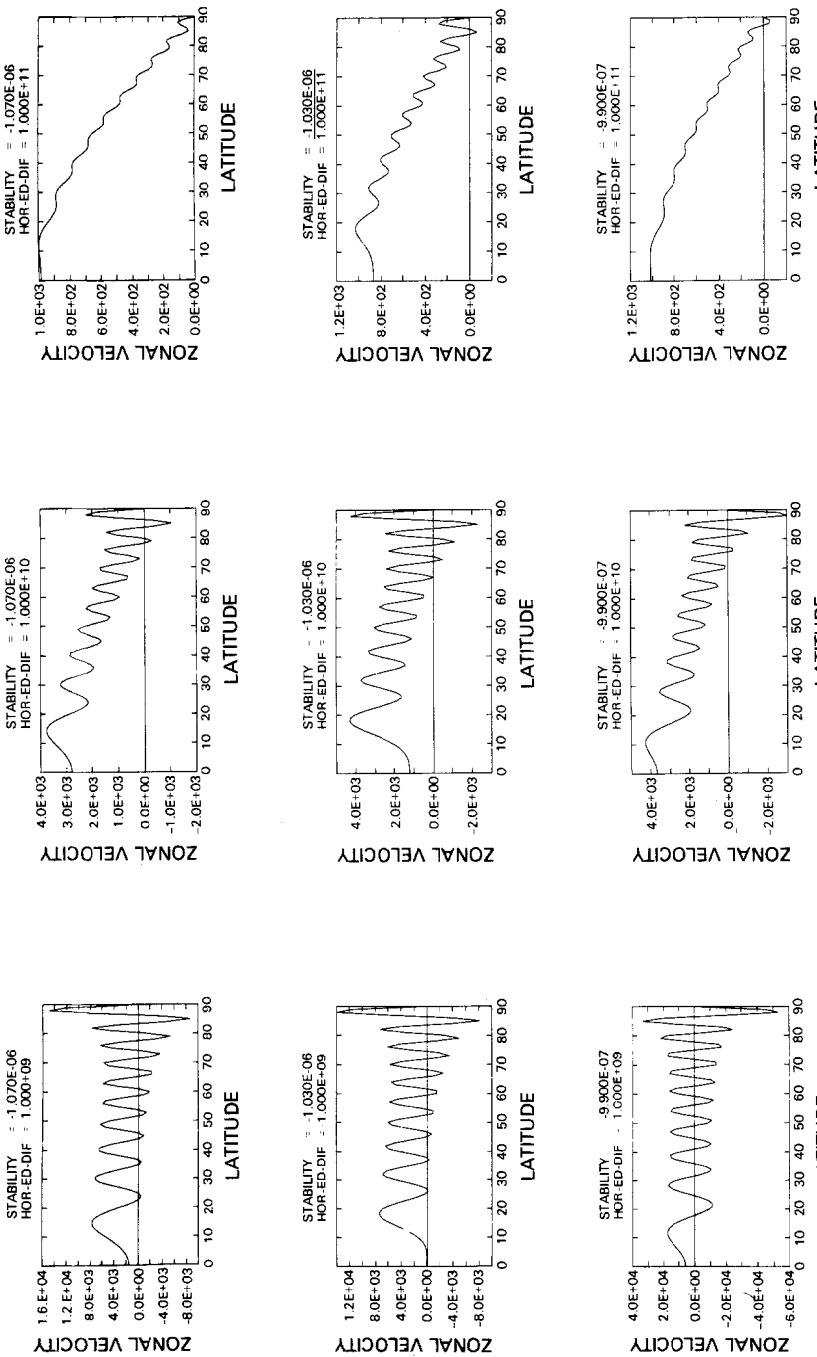

Fig. 8. For the values $R = 10^4$, 10^5, and 10^6, and for stabilities ranging from $S_0 = -9.9 \times 10^{-7}$ to -1.07×10^{-6}, the zonal velocity fields are shown as functions of latitude. Note that with the large R value on the right, where the resonance is very narrow, differential rotation is not important. With the smaller R value on the left, differential rotation prevails, but the equatorial region tends to corotate. An intermediate value satisfies the conditions observed on Jupiter; it also of the right order of magnitude to satisfy mixing length theory.

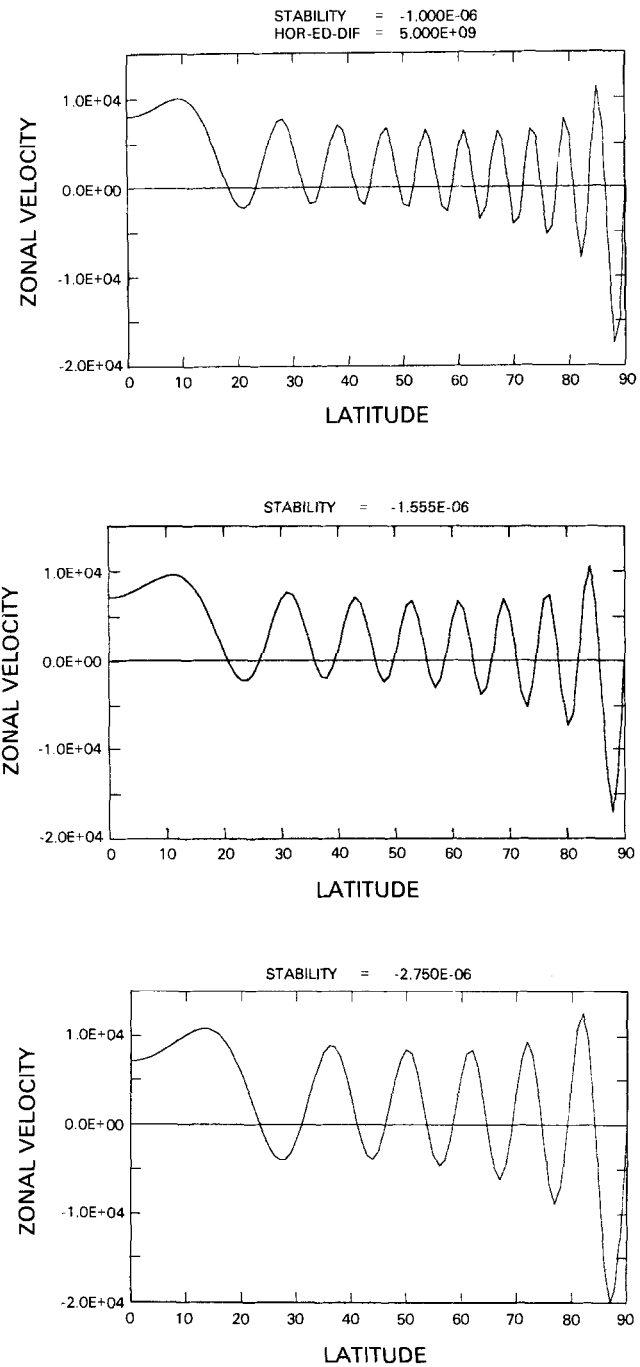

Fig. 9. For three values of stability, $S_0 = -1 \times 10^{-6}$, -1.55×10^{-6}, and -2.75×10^{-6}, each lying in a different 'resonance', the zonal velocity field is shown. The corresponding numbers of zonal jets are $n = 10$, 8, and 6 respectively which is consistent with the dependence (22), $n \propto 1/\sqrt{|S_0|}$.

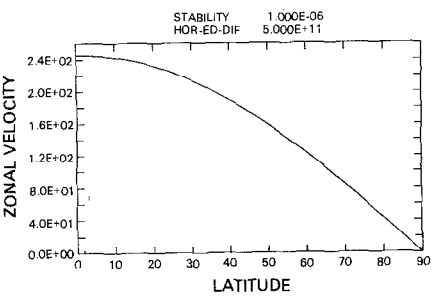
STABILITY 1.000E-06
HOR-ED-DIF 5.000E+11
ZONAL VELOCITY
2.4E+02
2.0E+02
1.6E+02
1.2E+02
8.0E+01
4.0E+01
0.0E+00
0 10 20 30 40 50 60 70 80 90
LATITUDE

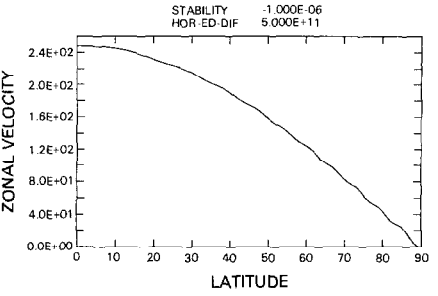
STABILITY -1.000E-06
HOR-ED-DIF 5.000E+11
ZONAL VELOCITY
2.4E+02
2.0E+02
1.6E+02
1.2E+02
8.0E+01
4.0E+01
0.0E+00
0 10 20 30 40 50 60 70 80 90
LATITUDE

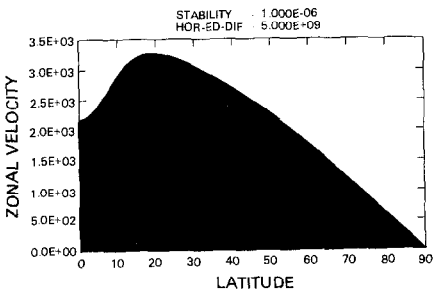
STABILITY 1.000E-06
HOR-ED-DIF 5.000E+09
ZONAL VELOCITY
3.5E+03
3.0E+03
2.5E+03
2.0E+03
1.5E+03
1.0E+03
5.0E+02
0.0E+00
0 10 20 30 40 50 60 70 80 90
LATITUDE

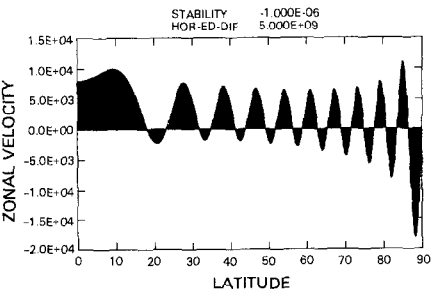
STABILITY -1.000E-06
HOR-ED-DIF 5.000E+09
ZONAL VELOCITY
1.5E+04
1.0E+04
5.0E+03
0.0E+00
-5.0E+03
-1.0E+04
-1.5E+04
-2.0E+04
0 10 20 30 40 50 60 70 80 90
LATITUDE

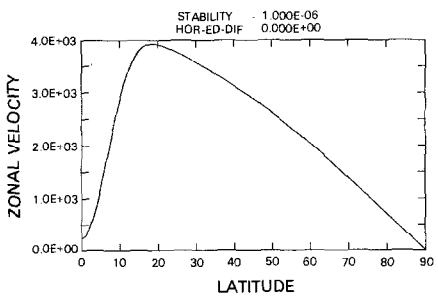
STABILITY 1.000E-06
HOR-ED-DIF 0.000E+00
ZONAL VELOCITY
4.0E+03
3.0E+03
2.0E+03
1.0E+03
0.0E+00
0 10 20 30 40 50 60 70 80 90
LATITUDE

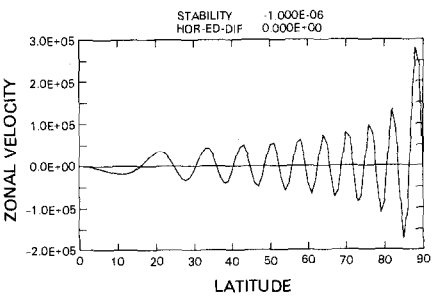
STABILITY -1.000E-06
HOR-ED-DIF 0.000E+00
ZONAL VELOCITY
3.0E+05
2.0E+05
1.0E+05
0.0E+00
-1.0E+05
-2.0E+05
0 10 20 30 40 50 60 70 80 90
LATITUDE

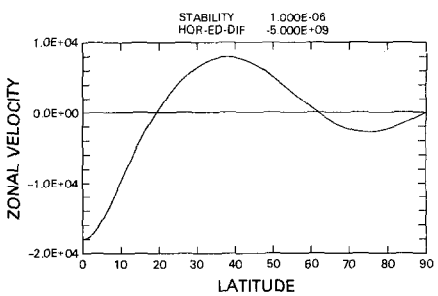
STABILITY 1.000E-06
HOR-ED-DIF -5.000E+09
ZONAL VELOCITY
1.0E+04
0.0E+00
-1.0E+04
-2.0E+04
0 10 20 30 40 50 60 70 80 90
LATITUDE

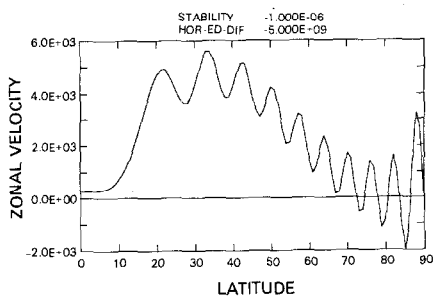
STABILITY -1.000E-06
HOR-ED-DIF -5.000E+09
ZONAL VELOCITY
6.0E+03
4.0E+03
2.0E+03
0.0E+00
-2.0E+03
0 10 20 30 40 50 60 70 80 90
LATITUDE

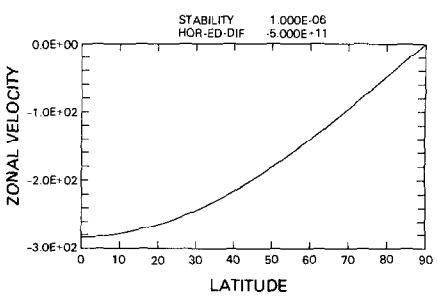
STABILITY 1.000E-06
HOR-ED-DIF -5.000E+11
ZONAL VELOCITY
0.0E+00
-1.0E+02
-2.0E+02
-3.0E+02
0 10 20 30 40 50 60 70 80 90
LATITUDE

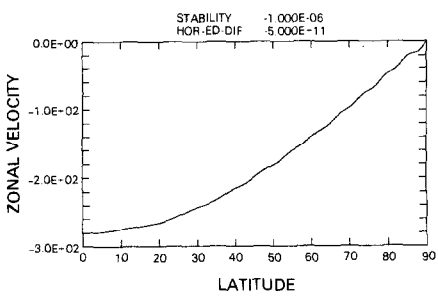
STABILITY -1.000E-06
HOR-ED-DIF -5.000E-11
ZONAL VELOCITY
0.0E-00
-1.0E-02
-2.0E-02
-3.0E-02
0 10 20 30 40 50 60 70 80 90
LATITUDE

We see from this analysis that, for certain values of negative stability (or certain values of $M_\Omega < 0$) one can *always* reproduce a large degree of differential rotation with positive and negative zonal jets. For large relative mixing factors, $R > 10^5$, however, this requires that the atmosphere is finely tuned to match a near resonance condition and this is not a likely scenario. For small mixing factors $R < 10^4$, when the width of the resonance is broad, differential rotation can be readily excited, virtually independent of the stability (M_Ω). However, as discussed earlier and seen from Figure 8, in the limit of small horizontal eddy diffusion, the equatorial region tends to corotate. This is not borne out by the observations of Jupiter and Saturn which show large equatorial jets.

Between these unrealistic extremes, rigid shell superrotation with small traces of zonal jets on one hand, and equatorial corotation with a large degree of differential rotation on the other hand, one can bracket the relative mixing factor: $10^4 < R < 10^5$. With this constraint, and considering mixing length theory which suggests $R = O(r^2/L^2h^2)$, we estimate that

$$R \sim \left(\frac{3r}{Lh}\right)^2 \tag{23}$$

would give reasonable results.

Under realistic conditions, the stability and scale height, for example, are changing continuously with altitude. Thus, the atmosphere will encounter one or more *broad* resonances with their positive and negative branches. The weight of each will depend on the heat source which also varies as a function of altitude. From such considerations it then seems clear that, with convective instability ($S_0 < 0$), various circulation patterns can be excited, including some that are dominated by the positive branch near a resonance. This is borne out by the earlier discussed numerical results for which we performed an integration in altitude.

We see from Figure 8 that the number of positive zonal jets does not depend on the relative mixing factor. The determining factor is the parameter M_Ω or the characteristic wave number L. This is demonstrated in Figure 9 where we examine the dependence on S_0 by going from one to another near resonance condition. Three values are chosen: $S_0 = -1 \times 10^{-6}$, -1.55×10^{-6}, and -2.75×10^{-6}, which produce equatorial jets of comparable magnitudes. Corresponding to these stabilities the numbers of positive jets over a

← Fig. 10. Retaining the vertical eddy diffusion coefficient $K_r(10^5)$ and the other parameters, the horizontal eddy diffusion coefficient K_θ is varied from 5×10^{11} through 0 to -5×10^{11}. In the left hand series the stability is positive, $S_0 = +10^{-6}$, in the right hand series it is negative, $S_0 = -10^{-6}$. For $K_\theta = 0$ in the middle, the zonal velocities are (near) zero at the equator. The small remnant velocity for positive stability is presumably due to truncation. For unrealistically large horizontal diffusion (top and bottom), this process dominates over vertical diffusion, and one obtains only a small rigid shell component of superrotation (with $K_\theta > 0$) or subrotation (with $K_\theta < 0$). The solutions which have some resemblence to observed planetary circulations are emphasized through shading, on the left Venus, on the right Jupiter. Note that the rotation rate of the planet is $\Omega = 1.8 \times 10^{-4}$. With the appropriate parameters for Venus the velocity would increase by about a factor of two and the equatorial minimum would be shallower, in closer agreement with the observations.

90° latitude range are $n = 10$, 8, and 6 respectively. Considering that $n \propto L$, and L is related to the stability through $M_L(S_0) = -1$, one obtains from Equation (20) the dependence $n \propto |S_0|^{-1/2}$, in close agreement with the results of Figure 9. For a fixed stability of $S_0 = -10^{-6}$, one can also demonstrate the influence of planetary rotation. The periods $\tau = 10$, 12.5, and 16.5 hr produce velocity fields (not shown) very similar to those in Figure 9. This is consistent with Equation (20) yielding $n \propto 1/\tau$. Provided $S_0 < 0$, the number of positive jets (over 90° latitude) is apparently $n \sim L/4 \propto |M_\Omega|^{-1/2} \propto r/(\tau\sqrt{|S_0|})$. The large rotation rate and radius of Jupiter as well as its small negative stability, all contribute to break up the zonal circulation into bands.

Finally, a study is presented in Figure 10 where we cover a wide range of parameters which may be of interest in the context of comparative planetary atmospheres. For the left hand series the stability is positive, $S_0 = +10^{-6}$; for the right hand series the stability is negative $S_0 = -10^{-6}$. The vertical eddy diffusion coefficient is fixed at $K_r = 10^5$. From the top panel down, the *horizontal* eddy diffusion coefficient decreases; the coefficient has a very large positive value in the top diagram and a very large negative value in the bottom diagram. For the panels in the middle the horizontal eddy diffusion coefficient is zero and the zonal velocity vanishes at the equator.

With very large horizontal diffusion (top and bottom), this process dominates over vertical diffusion in the momentum balance, and differential rotation cannot be maintained (except for a very narrow resonance, see Figure 7). Moreover, this process then diffuses the horizontal temperature contrast with the consequence that the rigid shell components of superrotation (for $K_\theta > 0$) or subrotation (for $K_\theta < 0$) are also small.

Under reasonable values of *positive* horizontal eddy diffusion, the results show zonal velocity fields, emphasized through shading, with characteristics similar to those observed on the planets. The right hand side resembles the banded wind field of Jupiter. The left hand side shows some similarity to the superrotation of Venus even though a rotation period of 10 hr and a very small stability are adopted. With parameters commensurate to Venus, the velocity increases by about a factor of two and the equatorial minimum is much shallower, in closer agreement with the observations.

In principle it is possible that the eddy transport processes are not diffusive and this might be simulated with equivalent negative diffusion coefficients. Our results suggest that a negative horizontal viscosity (diffusivity) is neither necessary nor appropriate to describe the circulations of Jupiter and Venus. However, for positive stability and small negative diffusion the equatorial region subrotates, and this scenario may be relevent for the Earth's lower atmosphere.

5.3. AGEOSTROPHIC FLOW

In their study of the Jovian circulation, Williams and Robinson (1973) had considered large eddy diffusion coefficients $K_r = 10^7$ and $K_\theta = 10^{13}\,\mathrm{cm^2\,s^{-1}}$. With these values, the magnitude of D_L (18) becomes comparable to that of M_L (17), and the atmosphere is no longer quasi-geostrophic. An ageostrophic resonance can then develop for

$$M_L + D_L \sim -1, \tag{24}$$

where

$$D_L = 0(1).$$

We follow the parametric study discussed in Figure 9, and adopt a stability $S_0 = -2.75 \times 10^{-6}$. Retaining the relative mixing factor $(K_\theta/K_r) = 5 \times 10^4$, we vary the eddy diffusion coefficients. Solutions of Equation (13) for the meridional and zonal velocities are presented in Figure 11. The top panel A shows the zonal velocity field which is identical to that in Figure 9. In panel B, K_r and K_θ are increased by a factor of 100 and, correspondingly, the zonal velocities decrease by the same amount. The meridional velocities and the *structure* of the zonal velocity field (number of positive jets), however, remain unchanged. For both panels A and B the resonance conditions are the same, since the eddy diffusion coefficients (due to heat conductivity and viscosity) exactly cancel in M_L. The parameter D_L is small and the meridional velocities are small compared to the zonal velocities (geostrophic). Proceedings to *C* and *D*, the horizontal eddy diffusion coefficient reaches $K_\theta = 10^{13}$, and the solutions change drastically. In C the zonal velocities are now comparable to the meridional component. The magnitude of D_L is comparable to that of M_L, and the geostrophic condition no longer holds. From C to D a relatively small increase of the diffusion coefficients is considered, yet the wind velocities increase by almost two orders of magnitude, indicating an ageostrophic resonance (24). To demonstrate that in this regime the latitudinal structure is primarily controlled by horizontal diffusion, another (near) resonance is described in E. Compared to D, we lower K_r by a factor of six while retaining nearly the same value for K_θ. Overall, the zonal velocity field retains its structure, but the magnitudes decrease by about a factor of three.

We note the differences between the geostrophic (A) and the ageostrophic (D) flow fields. From A to D, the magnitudes of the zonal velocity *decrease* by a factor of 100, while the magnitudes of the meridional velocity *increase* by about a factor of 10. For A the velocity fields extend all the way from the equator into the polar region, while for D they are confined to latitudes below 30°. Under the ageostrophic condition, our results are similar to those obtained by Williams and Robinson (1973). In this regime, the required outward flux of energy from the interior of Jupiter ($\propto K_r S_0$) is much too large as pointed out by Williams (1978). Moreover, there is no evidence to suggest that the magnitudes of the prevailing meridional wind field are comparable to those of the zonal component.

6. Conclusions

In the previous sections, we have taken two complementary approaches to study the dynamics of differential rotation (with application to Jupiter). In both we consider a linear spectral analysis (spherical harmonics) and parameterize the non-linear advections through anisotrophic eddy diffusion. One is a numerical model for which we obtain solutions by integrating over some altitude range of the atmosphere. The dimensions of this model are limited by the size (and speed) of the available computer. The number of

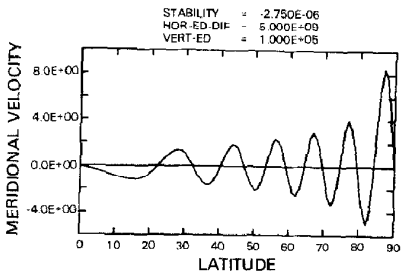
STABILITY = -2.750E-06
HOR-ED-DIF = 5.000E+09
VERT-ED = 1.000E+05
MERIDIONAL VELOCITY
8.0E+00
4.0E+00
0.0E+00
-4.0E+00
0 10 20 30 40 50 60 70 80 90
LATITUDE

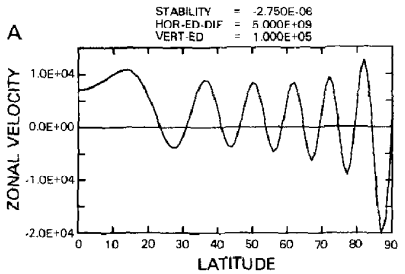
A
STABILITY = -2.750E-06
HOR-ED-DIF = 5.000E+09
VERT-ED = 1.000E+05
ZONAL VELOCITY
1.0E+04
0.0E+00
-1.0E+04
-2.0E+04
0 10 20 30 40 50 60 70 80 90
LATITUDE

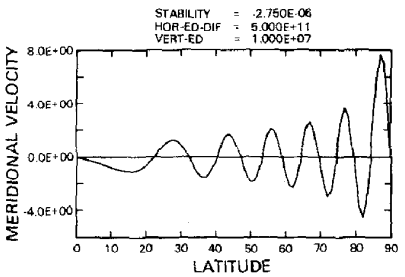
STABILITY = -2.750E-06
HOR-ED-DIF = 5.000E+11
VERT-ED = 1.000E+07
MERIDIONAL VELOCITY
8.0E+00
4.0E+00
0.0E+00
-4.0E+00
0 10 20 30 40 50 60 70 80 90
LATITUDE

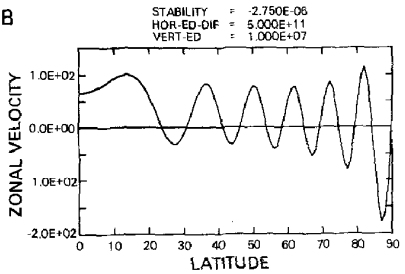
B
STABILITY = -2.750E-06
HOR-ED-DIF = 5.000E+11
VERT-ED = 1.000E+07
ZONAL VELOCITY
1.0E+02
0.0E+00
-1.0E+02
-2.0E+02
0 10 20 30 40 50 60 70 80 90
LATITUDE

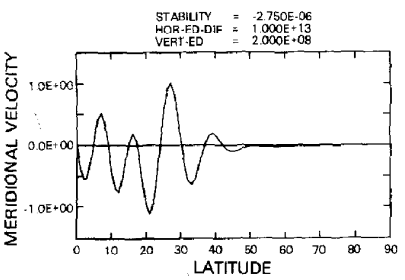
STABILITY = -2.750E-06
HOR-ED-DIF = 1.000E+13
VERT-ED = 2.000E+08
MERIDIONAL VELOCITY
1.0E+00
0.0E+00
-1.0E+00
0 10 20 30 40 50 60 70 80 90
LATITUDE

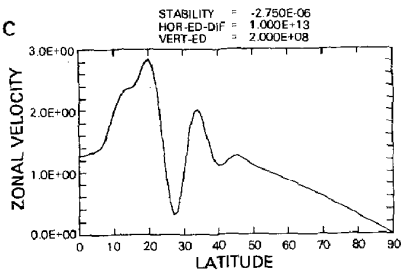
C
STABILITY = -2.750E-06
HOR-ED-DIF = 1.000E+13
VERT-ED = 2.000E+08
ZONAL VELOCITY
3.0E+00
2.0E+00
1.0E+00
0.0E+00
0 10 20 30 40 50 60 70 80 90
LATITUDE

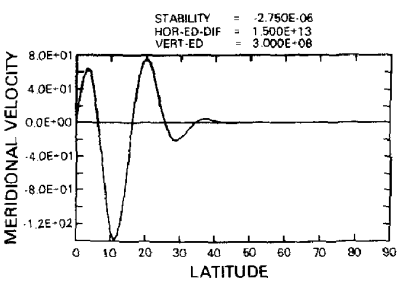
STABILITY = -2.750E-06
HOR-ED-DIF = 1.500E+13
VERT-ED = 3.000E+08
MERIDIONAL VELOCITY
8.0E+01
4.0E-01
0.0E+00
-4.0E-01
-8.0E-01
-1.2E-02
0 10 20 30 40 50 60 70 80 90
LATITUDE

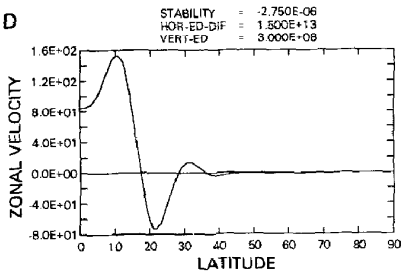
D
STABILITY = -2.750E-06
HOR-ED-DIF = 1.500E+13
VERT-ED = 3.000E+08
ZONAL VELOCITY
1.6E+02
1.2E+02
8.0E+01
4.0E+01
0.0E+00
-4.0E+01
-8.0E+01
0 10 20 30 40 50 60 70 80 90
LATITUDE

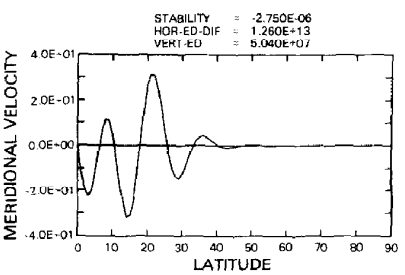
STABILITY = -2.750E-06
HOR-ED-DIF = 1.260E+13
VERT-ED = 5.040E+07
MERIDIONAL VELOCITY
4.0E-01
2.0E-01
0.0E+00
-2.0E-01
-4.0E-01
0 10 20 30 40 50 60 70 80 90
LATITUDE

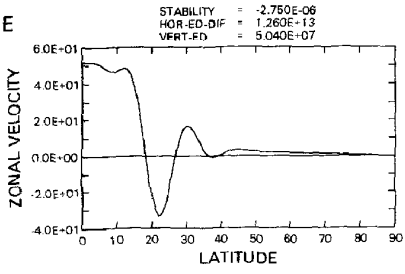
E
STABILITY = -2.750E-06
HOR-ED-DIF = 1.260E+13
VERT-ED = 5.040E+07
ZONAL VELOCITY
6.0E+01
4.0E+01
2.0E+01
0.0E+00
-2.0E+01
-4.0E+01
0 10 20 30 40 50 60 70 80 90
LATITUDE

modes considered may be insufficient to provide the latitudinal resolution, and the altitude range is probably not large enough to cover the depth of the Jovian circulation. Our second approach represents a semianalytical, one-layer model in which the vertical structure of the atmosphere is parameterized. In this model, however, the latitudinal structure can be fully resolved by considering a large number of modes. Here, the computational effort is minimal and permits parametric studies that provide insight into different regimes. Although these models have different limitations, they produce similar results under similar conditions.

We consider solar differential heating at low latitudes as the principal source for driving the circulation. In the geostrophic regime, the dimensionless parameter M_Ω, defined in (21), essentially determines the latitudinal structure of the meridional flow. A single Hadley cell develops for $M_\Omega > 0$, when the atmosphere is convectively stable ($S_0 > 0$). In an atmosphere which is convectively unstable (Jupiter and Saturn, presumably), the transport processes, on one hand due to linear global scale advections of energy ($\propto WS_0$) and planetary angular momentum (Coriolis force), and on the other hand due to eddy diffusion from smaller scale non-linear advections, can nearly balance each other. Depending on S_0, this condition develops preferentially at or near a particular latitudinal wave number which in turn characterizes the motions. Thus, a multi-cellular meridional circulation developes. Our estimate of the negative stability, on the order $S_0 \sim -10^{-6}$ K cm^{-1} and too small to be observed directly, is primarily determined by the observed latitudinal structure of the Jovian circulation. In the geostrophic regime, this estimate and the magnitude of the meridional flow do not depend on the eddy diffusion. Through mixing length theory, the eddy diffusion coefficients, however, are determined by the meridional winds.

The efficiency of the meridional circulation in driving the zonal wind field and temperature variations depends primarily on the eddy diffusion coefficients. For the given solar driving, and with a fixed relative mixing factor R, the computed zonal velocities vary as $\propto (\Delta q/K)$. On that basis we determine $K_r \sim 3 \times 10^5$ cm^2 s^{-1} (near the one bar pressure level). Considering our estimated negative stability, this is also the right order of magnitude to match the observed upward flux of energy from the planetary interior, $F \propto K_r S_0$ (Equation (3)). Moreover, based on our computed vertical velocities of about 3×10^{-2} cm s^{-1} (not shown), mixing length theory yields a similar magnitude of about $K_r \sim WH \sim 1.5 \times 10^5$.

In describing the zonal circulation and temperature variations, the relative mixing

Fig. 11. An analysis is presented illustrating the characteristics of the ageostrophic flow ($D_L \sim 1$). A stability $S_0 = -2.75 \times 10^{-6}$ is adopted along with the other parameters from Figure 9. For the panels A through D, the relative mixing factor is fixed at $K_\theta/K_r = 5 \times 10^4$, while the magnitudes of the diffusion coefficients are increased as indicated in the figure. For A and B, the meridional velocities are the same, but the zonal velocities differ by the difference in the eddy diffusion coefficients. In C the flow becomes ageostrophic and the circulation changes drastically. In panels D and E ageostrophic velocity fields are shown for near resonance conditions. Here the zonal and meridional components are of comparable magnitudes.

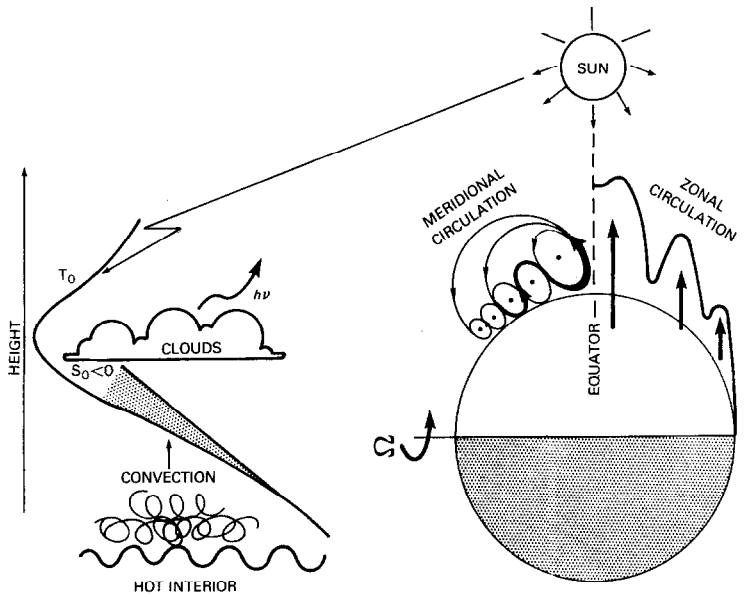

Fig. 12. The important elements of the model are summarized in schematic form. On average, the troposphere is weakly convectively unstable; a small superadiabatic temperature lapse rate maintains the upward transport of heat from the planetary interior. Above the tropopause the solar heat input dominates and energy is conducted downwards. The atmosphere is preferentially heated by solar radiation at low latitudes; motions are rising near the equator and falling at higher latitudes. Under conditions of convective instability, the upward motions are capable of funneling energy into the equatorial region which is conducive to the formation of an equatorial jet. At the same time, energy transport by eddy diffusion and global scale advection tend to balance each other, and the meridional circulation is broken up into a large number of smaller cells. Concomitantly, a banded wind field develops in the zonal component. With the adopted eddy diffusion coefficients which are consistent with mixing length theory, the flow is nearly geostrophic.

factor $R = (K_\theta/K_r)$ is of critical importance. If this value is too small, the equatorial region tends to corotate; if it is too large, differential rotation – and under more extreme conditions even regid shell superrotation – cannot be maintained, except near a narrow resonance (associated with a narrow range of stabilities), which is an unlikely scenario. The intermediate value of $R \sim 5 \times 10^4$ is consistent with the observations on Jupiter and just of the right order of magnitude to obey mixing length theory.

Summarizing these results it appears that our working hypothesis about eddy diffusion is internally consistent.

For our understanding of the Jovian circulation it is of critical importance that the troposphere is weakly convectively unstable (Figure 12) and that the eddy diffusion coefficients are sufficiently small to permit geostrophic flow. That the flow is geostrophic is a conclusion, not an a priori assumption. Under this condition, the meridional circulation is multi-cellular and of the Ferrel–Thomson type, which is consistent with the observed striation in the clouds. Under solar driving, the magnitudes of the computed vertical and meridional velocities, although small, can maintain zonal jets of about 10^4cm s^{-1},

provided the adopted eddy diffusion coefficients are also relatively small which in turn is consistent with mixing length theory.

In the stable stratosphere at higher altitudes the rigid shell component of superrotation dominates. The zonal velocity field 'degenerates', and a single, broad positive jet develops at mid latitudes. This wind field has some similarity with the observed superrotation in the cloud cover of Venus.

Considering the heuristic nature of our models, with the linearizations, and the simplifying assumptions about eddy diffusion, Prandtl number, radiative cooling and solar driving, we cannot attribute much significance to some of the details in the results. There is no evidence that large jets are observed in the polar region such as shown in Figure 4. In a realistic atmosphere of sufficient depth, where the stability (or M_Ω) changes over a wide range, several convective eigenmodes (near resonances), with their positive and negative branches (e.g. Figures 5 and 8), can be excited. Their superposition, due to vertical transport processes, tends to cancel perferentially the zonal jets at higher latitudes, while amplifying the jets near the equator. On this basis one should expect a rich variety of phenomena in the observed atmospheric circulation patterns, and we suggest that, to some extent, the large differences between Jupiter and Saturn are such manifestations.

The computed latitudinal temperature variations show plateaus similar to those observed on Jupiter (Hanel *et al.*, 1979a, b). However, our amplitudes in the numerical model are too large by about a factor of three. This may indicate that the prevailing circulation goes deeper than our numerical approach allows us to go; it may also be due to our simplifying assumptions about the Prandtl number and the height dependences in eddy diffusion and radiative cooling. These problems, however, should not alter significantly our principle conclusions.

Acknowledgement

We are indepted to B. J. Conrath and R. E. Hartle (both GSFC) for helpful discussions and to D. R. Stevens-Rayburn (Applied Research Corporation) and F. Varosi (Science Applications Research) for assistance in the analysis.

References

Biermann, L.: 1951, *Zeitschrift für Astrophysik* **28**, 304.

Chan, K. L., Sofia, S. and Wolff, C. L.: 1982, *Astrophys, J.* **263**, 935.

Chapman, S. and Lindzen, R. I.: 1970, *Atmospheric Tides*, D. Reidel Publ. Co., Dordrecht, Holland.

Durney, B. R. and Roxburgh, I. W.: 1971, *Solar Phys.* **16**, 3.

Gierasch, P. J.: 1975, *J. Atm. Sci.* **32**, 1038.

Hanel, R., Conrath, B., Flasar, M., Kunde, V., Lowman, P., Maguire, W., Pearl, J., Pirraglia, J., Samuelson, R., Gautier, D., Gierasch, P., Kumar, S. and Ponnamperuma, C.: 1979a, *Science* **204**, 972.

Hanel, R., Conrath, B., Flasar, M., Herath, L., Kunde, V., Lowman, P., Maguire, W., Pearl, J., Pirraglia, J., Samuelson, R., Gautier, D., Gierasch, P., Horn, L., Kumar, S. and Ponnamperuma, C.: 1979b, *Science* **206**, 952.

Held, I. M. and Hou, A. Y.: 1980, *J. Atm. Sci.* **37**, 515.

Hide, R.: 1969, *J. Atm. Sci.* **26**, 841.

Mayr, H. G. and Harris, I.: 1983, *Astron. and Astrophys.* **121**, 124.

Morse, P. M. and Feshbach, H.: 1953, *Methods of Theoretical Physics*, McGraw-Hill Book Co., New York.

Orton, G. S. and Ingersoll, A. P.: 1976, *The Thermal Structure and H_e–H_2 ratio, Jupiter*, University of Arizona Press, Tucson, Arizona.

Rüdiger, G.: 1980, *Geophys. Astrophys. Fluid Dynamics* **16**, 239.

Schubert, G., Covey, C., Del-Genio, A., Elson, L. S., Keating, G., Seiff, A., Young, R. E., Apt, J., Counselman III, C. C., Kliore, A. J., Limaye, S. S., Revercomb, H. E., Stromovsky, L. A. Suomi, V. E. Taylor, F., Woo, R. and Von Zahn, U.: 1980, *J. Geophys. Res.* **85**, 8007.

Smith, B. A., Soderblom, L. A., Johnson, T. V., Ingersoll, A. P., Collins, S. A., Schoemaker, E. M., Hunt, G. E., Masursky, H., Carr, M. H., Davies, M. E., Cook II, A. F., Boyce, J., Danielson, G. E., Owen, T., Sagan, C., Feebe, R. F., Veverka, J., Strom, R. G. McCauley, J. F., Morrison, D., Briggs, G. A. and Suomi, V. E.: 1979a, *Science* **204**, 951.

Smith, B. A., Soderblom, L. A., Beebe, R., Boyce, J., Briggs, G., Carr, M., Collins, S. A., Cook II, A. F., Danielson, G. E., Davies, M. E., Hunt, G. E., Ingersoll, A., Johnson, T. V., Masursky, H., McCauley, J., Morrison, D., Owen, T., Sagan, C., Schoemaker, E. M., Strom, R., Suomi, V. E. and Veverka, J.: 1979b, *Science* **206**, 927.

Smith, B. A., Soderblom, L., Beebe, R., Boyce, J., Briggs, G., Bunker, A., Collins, S. A., Hansen, C. J., Johnson, T. V., Mitchell, J. L., Terrile, R. J., Carr, M., Cook II, A. F., Cuzzi, J., Pollak, J. B., Danielson, G. E., Ingersoll, A., Davies, M. E., Hunt, G. E., Masursky, H., Schoemaker, E., Morrison, D., Owen, T., Sagan, C., Veverka, J., Strom, R. and Suomi, V. E.: 1981, *Science* **212**, 163.

Volland, H. and Mayr, H. G.: 1972a, *J. Atm. Terr. Phys.* **34**, 1725.

Volland, H. and Mayr, H. G.: 1972b, *Space Res.* **12**, 1095.

Wallace, L., Prather, M. and Belton, M. J. S.: 1974, *Astrophys. J.* **193**, 481.

Williams, G. P.: 1978, *J. Atm. Sci.* **35**, 1399.

Williams, G. P. and Robinson, J. B.: 1973, *J. Atm. Sci.* **30**, 684.